International Journal of Pharmaceutics: X 6 (2023) 100199

Contents lists available at ScienceDirect

International Journal of Pharmaceutics: X

journal homepage: www.sciencedirect.com/journal/international-journal-of-pharmaceutics-x

Preparation of chitosan-coated hollow tin dioxide nanoparticles and their application in improving the oral bioavailability of febuxostat

Junpeng Sun [a], Jiaqun Du [a], Xiaobang Liu [a], Jinyu An [a], Yingqiao Li [a], Yanan Yu [b], Minghui Li [c], Li Zheng [a], Chao Wu [a,*], Lili Hu [a,*]

[a] Pharmacy School, Jinzhou Medical University, Jinzhou, Liaoning 121001, China
[b] Medical College of Jinzhou Medical University, Jinzhou Medical University, 121010, China
[c] Jinzhou Medical University, Jinzhou, Liaoning 121001, China

ARTICLE INFO

Keywords:
Febuxostat
Tin dioxide
Chitosan
Saturation solubility
Dissolution rate
Oral bioavailability
Intestinal tract

ABSTRACT

The aim of this study was to design a chitosan-coated hollow tin dioxide nanosphere (CS-HSn) for loading febuxostat (FEB) using an adsorption method to obtain a sustained-release system (CS-HSn-FEB) to improve the oral bioavailability of FEB. The morphological characteristics of hollow tin dioxide nanospheres (HSn) and CS-HSn were analyzed by transmission electron microscopy (TEM) and dynamic light scattering (DLS). The hemolysis test and CCK-8 test were used to assess the biosafety of HSn and CS-HSn. Powder X-ray diffraction (PXRD) and differential scanning thermal analysis (DSC) were performed on CS-HSn-FEB to analyze the drug presence status. The dissolution behavior and changes in plasma drug concentration of CS-HSn-FEB were evaluated in vitro and in vivo. Sections of intestinal tissues from SD rats were obtained to observe whether chitosan could increase the distribution of nanoparticles in the intestinal tissues. The results showed that FEB was present in CS-HSn in an amorphous state. Moreover, CS-HSn, with good biosafety, significantly improved the water solubility and oral absorption of FEB, indicating that CS-HSn has great potential to improve the intestinal absorption and oral bioavailability of insoluble drugs.

1. Introduction

Gout is a recurrent inflammatory disease caused by the deposition of uric acid in the form of monosodium urate (MSU) in synovial membranes, bursae, cartilage and other tissues (Dehlin et al., 2020; Major et al., 2018). Patients have only intermittent or persistent hyperuricemia during asymptomatic periods, and during gout attacks, patients may present with acute gouty arthritis, gout stones, and chronic arthritis with clinical manifestations of renal lesions (Li et al., 2019). The current clinical treatment for hyperuricemia and gout is mainly to reduce the blood uric acid level in the body to prevent joint damage and protect renal function (Nuki and Simkin, 2006). A commonly used drug is allopurinol. However, it has serious side effects, such as Stevens-Johnson syndrome (SJS) (Gupta et al., 2019; Huong et al., 2022; Liao et al., 2021). Febuxostat (FEB), unlike allopurinol, is a novel nonpurine selective inhibitor of xanthine oxidase that can inhibit uric acid synthesis and shows good therapeutic effects for hyperuricemia and gout (Huong et al., 2022). Although FEB has received much attention among antihyperuricemia drugs (Becker et al., 2005), its low water solubility (below 0.0129 mg/mL) leads to poor gastrointestinal bioavailability, limiting its widespread use (Londhe and Bakshi, 2023; Habib et al., 2021). In recent years, many pharmaceutical methods using nanoporous materials have attracted much attention from researchers to improve the solubility and bioavailability of insoluble drugs (Foote, 2007; Zhang et al., 2022). For example, commonly used mesoporous materials include mesoporous TiO2 nanofibers (Lou et al., 2019), mesoporous silica (Tang et al., 2012), nanoporous carbon (Ejsmont et al., 2021), nanoporous inorganic films (Li et al., 2020), and mesoporous tin dioxide (Yang et al., 2022). Compared with other materials, mesoporous tin dioxide, as a metal oxide nanocarrier, has promising applications as a potential pharmaceutical excipient. Andi Bai et al. (Bai et al., 2018) used tin dioxide with a mesoporous structure to improve the oral relative bioavailability of fenofibrate, and the results showed that tin dioxide has great potential in improving the aqueous solubility and enhancing the bioavailability of insoluble drugs. In this study, we prepared hollow tin dioxide (HSn) nanocarriers by a hydrothermal synthesis method. In

* Corresponding author.
E-mail addresses: wuchao@jzmu.edu.cn (C. Wu), hulili19860415@163.com (L. Hu).

https://doi.org/10.1016/j.ijpx.2023.100199
Received 30 May 2023; Received in revised form 7 July 2023; Accepted 8 July 2023
Available online 13 July 2023

contrast to other forms of tin dioxide, HSn has a unique hollow structure that results in in a lower density and higher loading capacity (Zhao et al., 2022a, 2022b). The nanoscale spatial confinement effect of HSn has significantly improved the water solubility and dissolution rate of insoluble drugs (Zhou et al., 2021; Ibrahim et al., 2020), but problems of oral burst release and gastrointestinal environmental impacts remain (Sun et al., 2020). Therefore, it is necessary to modify the surface of HSn to effectively regulate drug release and improve the oral absorption of the drug.

Chitosan (CS), a natural polycationic polysaccharide with a large number of amino groups (Bernkop-Schnürch and Dünnhaupt, 2012; Wang et al., 2008), can act as an active site for enhancing cell and nanoparticle adhesion (Bonferoni et al., 2009; Hu et al., 2012). It has also been reported that CS can open the tight junctions of epithelial cells to increase the retention and transportation of nanoparticles on the mucosal surface (Dou et al., 2019; Sahni et al., 2008), thereby improving the gastrointestinal absorption of insoluble drugs. This not only shows the excellent transfer and adhesion properties of CS in the human gastrointestinal tract but also effectively prevents drug inactivation and degradation caused by gastrointestinal enzymes and low pH values (Kimura et al., 2001; Hu et al., 2010; Tong et al., 2020). Therefore, CS is widely used as a functional material for oral drug formulations and has great promise in improving the gastrointestinal absorption of drugs and enhancing the oral bioavailability of insoluble drugs.

In this study, a nano-slow-release system (CS-HSn-FEB) successfully equipped with FEB was prepared by coating HSn with CS and using FEB as a model drug. FEB was found to be present in the amorphous state in CS-HSn. Compared with HSn, CS-HSn exhibited superior cellular internalization and higher intestinal absorption in vivo. CS-HSn-FEB also showed better therapeutic effects in alleviating high uric acid levels in rats. Thus, CS-HSn, as a novel and safe nanocarrier, provides a new strategy for reducing uric acid levels.

2. Materials and methods

2.1. Materials

Deionized water (homemade), febuxostat (purity ≥98%, Shanghai Dibo Biotechnology Co., Ltd.) anhydrous ethanol (Tianjin Xinbote Chemical Co. Ltd.), urea (Tianjin Yongsheng Fine Chemical Co. Ltd.), acetonitrile (Tianjin Damao Chemical Reagent Factory), and potassium stannate trihydrate were purchased from Aladdin Industrial Company (Shanghai, China). 3-Aminopropyltriethoxysilane (APTES) was purchased from Aladdin Industrial Corporation (Shanghai, China). Hematoxylin-eosin/HE staining kits were purchased from Beyotime Biotechnology Co. Chitosan, dimethicone, tetrahydrofuran, formic acid, and heparin were purchased from Sinopharm Chemical Reagent Co. Ltd.

2.2. The synthesis of HSn and CS-HSn

2.2.1. Preparation of hollow tin dioxide (HSn) and amine-based functionalization of HSn (HSn-NH_2)

First 120 mL of an aqueous solution containing 50% ethanol was prepared. Then, 168 mg of $K_2SNO_2 \bullet 3H_2O$ was accurately weighed into the above solution and stirred until dissolved, followed by 720 mg of urea, which was stirred until dissolved. The above solution was transferred to the reaction kettle, heated at 150 °C for 24 h, removed from the reaction kettle, cooled, centrifuged to collect the precipitate, washed with water three times, and washed with alcohol three times, then vacuum dried and collected for later use. Amino functionalization: First, 500 mg of the above HSn powder was dried in a round bottom flask in an oil bath (100 °C) for 20 min and cooled to room temperature. Then, 2 mL of APTES was dissolved in 50 mL of ethanol, and nitrogen gas was introduced to obtain a nitrogen-filled system. The round bottom flask was then connected to a reflux condenser and refluxed at 77 °C for 10 h. The flask was cooled, centrifuged, washed 3 times with anhydrous ethanol, and then dried under vacuum.

2.2.2. Preparation of chitosan-coated tin dioxide (CS-HSn)

CS (0.15% *W/V*)/was prepared in a 10% *V*/V acetic acid solution, and the pH was adjusted to 6.0 with 1 M NaOH. Then, 40 mL of CS/acetic acid solution with a pH of 6.0 was added to 0.35 g of solid tin dioxide and stirred at room temperature for 36 h. After the reaction, the product was centrifuged, washed twice with deionized water, and vacuum-dried at room temperature to obtain CS-HSn (Ghahfarokhi et al., 2022).

2.2.3. Preparation of CS-HSn drug-loaded nanoparticles (CS-HSn-FEB)

The selected model drug was FEB, which is a poorly soluble drug that is usually dissolved in an organic solvent and loaded by the adsorption equilibrium method. First, 0.3 g of FEB was precisely weighed and dissolved in 1 mL of tetrahydrofuran. After fully dissolving, 0.15 g of CS-HSn solid powder was weighed, and the above solution was added. The mixture was then incubated overnight with stirring and centrifuged. The pellet was removed and vacuum dried.

2.3. Encapsulation efficiency

To quantify the amount of encapsulated FEB, certain amounts of CS-HSn-FEB and HSn-FEB drug powders were taken and dissolved in quantitative acetonitrile as the FEB extraction solvent, then centrifuged at 8000 rpm for 10 min. The supernatant was removed and passed through a 0.22 μm filter. The FEB concentration in the carrier was determined at 315 nm using a UV spectrophotometer (UV-757CRT, Shanghai Precision Scientific Instrument Co., Ltd., Shanghai, China).

Encapsulation efficiency (%) = (weight of loaded FEB/weight of FEB in feed) × 100%.

2.4. Characterization of HSn-FEB and CS-HSn-FEB

The particle size and morphology of HSn-FEB and CS-HSn-FEB were observed using transmission electron microscopy (TEM, JEM-2100, JEOL, Tokyo, Japan) and dynamic light scattering (DLS). We used an X-ray diffractometer (Rigaku Geigerflex XRD, Company, Japan, 30 kV and 30 mA Philips) and performed differential scanning calorimetry (DSC) using a differential scanning calorimeter (DSC-60, Shimadzu, Japan) from 30 °C to 300 °C at 10 °C/min under N_2. The flow rate was 150 mL/min. Scan for pure FEB, CS-HSn, CS-HSn-FEB, and physical mixture of FEB and CS-HSn (PM).

2.5. In vitro release of FEB

To investigate the in vitro drug release behavior, three drug powders, FEB, HSn-FEB, and CS-HSn-FEB, were uniformly dispersed in PBS (pH = 7.4) and transferred into dialysis bags, which were placed in the release medium and slowly stirred at 100 rpm in a 37 °C water bath. At predetermined time intervals, the dissolution medium (3 mL) was collected for filtration and supplemented with the same volume of PBS to maintain a constant dissolution volume. The sample solution was passed through a 0.22 μm microporous filter membrane. The absorbance of the samples was measured at 315 nm using a UV spectrophotometer. The cumulative release rate was calculated, and the release curve was plotted.

2.6. In vitro cell assay

2.6.1. Cell culture

The Caco-2 cell line was cultured using DMEM, which consisted of 10% fetal bovine serum (Hy Clone), 100 U/mL penicillin, and 100 μg/mL streptomycin (Gibco). The medium was changed every two days, and cells were passaged using trypsinization.

2.6.2. Cell viability assay (Caco-2 cell)

In vitro cytotoxicity assessment of HSn and CS-HSn in Caco-2 cells by CCK-8 assay. Caco-2 cells were seeded in 96-well plates at a concentration of 5×10^3 cells per well and cultured at 37 °C for 24 h. Then, different concentrations (1000, 500, 250, 100, 50, 10, 5 ng/mL) of HSn and CS-HSn were suspended in the medium. To determine the biosafety of HSn and CS-HSn, different concentrations of the suspension (1000, 500, 250, 100, 50, 10, and 5 ng/mL) were added to 96-well plates. Cells were incubated for 24 h, and then 10 μL of CCK-8 solution was added to each well and incubated for 4 h in the dark. The OD value at 490 nm was measured by recording the absorbance intensity at 450 nm (Versa Max, Molecular Devices, Sunnyvale, CA, USA) on a microplate reader. Cell viability was calculated using the following formula: Cell viability = $OD_t/OD_c \times 100\%$.

where OD_t represents the absorbance of the treated cells, and OD_c represents the absorbance of the control cells.

2.6.3. Cellular internalization of nanoparticles

The internalization of different nanoparticles by Caco-2 cells was observed by confocal fluorescence microscopy (CLSM). HSn-NH_2 (100 mg) and CS-HSn (100 mg) were added to the above solution with 1 mg/mL FITC ethanol solution. The solutions were stirred for 4 h and dried by centrifugation to obtain FITC-labeled HSn-FITC and CS-HSn-FITC. Subsequently, Caco-2 cells were seeded in confocal discs and cultured for 48 h. The cells were incubated with 100 μg/mL HSn-FITC and CSn-FITC suspensions for 40 min at 37 °C. Cells were fixed with 4% paraformaldehyde solution for 30 min, permeabilized with 0.1% Triton for 15 min, and then blocked with goat serum for 2 h. Staining was performed by incubating with rhodamine-labeled ghost pen cyclic peptide (rhodamine-phalloidin) for 15 min and incubating with DAPI for 15 min. Optical images of nanoparticle distribution in Caco-2 cells were obtained using CLSM.

2.7. In vivo experiment

2.7.1. Animals

Healthy SD rats (300 ± 50 g) were provided by the Experimental Animal Center of Jinzhou Medical University. All animal experiments in this study were approved by the Experimental Animal Ethics Committee of Jinzhou Medical University.

2.7.2. Pharmacokinetic study in SD rats

This experiment was used to predict the in vivo drug release properties of FEB, HSn-FEB and CS-HSn-FEB. Rats were fasted for 12 h prior to the experiment but were allowed to drink freely throughout the test period. Nine SD rats were randomly divided into three groups of three rats each. FEB, HSn-FEB and CS-HSn-FEB were administered orally (administration method: gavage; dose administered: equivalent to febuxostat content of 10 mg/kg). Orbital blood sampling was performed at 0, 0.25, 0.5, 1, 2, 4, 6, 8, 12, and 24 h after oral administration using heparin-treated centrifuge tubes with a blood sample volume of approximately 0.5 mL. After centrifugation at 5000 rpm for 10 min, the supernatant was removed, and plasma was obtained. The plasma samples were stored in a refrigerator at −20 °C for backup, and the blood drug concentrations were determined by HPLC (Shimadzu LC-2030). The mobile phase was acetonitrile/0.1% formic acid aqueous solution (61/39, *v*/v) at a flow rate of 1.0 mL/min with a detection wavelength of 315 nm, and the injection volume was 20 μL. The pharmacokinetic parameters were calculated using Pksolver version 2.0.

2.7.3. In vivo CS-HSn uptake efficiency

To verify the in vivo distribution effect of CS-HSn, HSn was used as a control. FITC-labeled HSn (5 mg/kg) and CS-HSn (5 mg/kg) were injected via the tail vein. Mice were sacrificed after 2 h, intestinal tissues and organs (heart, liver, spleen, lung and kidney) were removed, and fluorescence distribution images of HSn and CS-HSn were tracked with a Bruker In vivo FX Pro (In vivo FX-Pro, Billerica, MA).

2.7.4. Intestinal distribution of the functional nanocarriers

Fluorescence microscopy was used to observe the distribution of FITC-labeled nanoparticles in the intestine. SD rats were fasted for 12 h before the experiment, and the whole experiment was performed without direct light. Subsequently, the modified nanoparticle was administered orally by gavage (10 mg/kg). After a period of time, the rats were sacrificed, and the duodenum, ileum and jejunum of intestinal tissue were harvested. The tissues were fixed and dehydrated in 4% PFA, 10% sucrose solution, 20% sucrose solution, and 30% sucrose solution. The tissue was then frozen and embedded in cryogenic medium (OCT), and 8 μm tissue sections were cut using a cryosectioning instrument (CM3050S, Leica) and attached to glass slices. The sections were washed three times with PBS, fixed with 4% paraformaldehyde for 10 min, and washed three times with PBS. Nuclei were stained with DAPI, and F-actin was stained with rhodamine-phalloidin. Fluorescence microscopy was used to observe the distribution of each segment at different time periods before and after modification.

2.7.5. Rat model of hyperuricemia and drug administration

The hyperuricemic rat model was established by intraperitoneal injection of potassium oxyzincate (25 mg/mL, 10 mL/kg) and gavage of hypoxanthine premix (100 mg/mL, 10 mL/kg). Except for the normal group, the above methods were used to establish the hyperuricemia model in all the groups. Briefly, 1 h after the establishment of the model, the normal and hyperuricemic experimental groups received saline (2 mL), while the rest of the groups were given the corresponding therapeutic drugs. Then, at set time points (0 h, 1 h, 2 h, 4 h, 6.5 h, 9 h and 12 h), blood was collected from the fundus vein with the use of a uric acid test kit to determine serum uric acid levels.

2.7.6. Hematoxylin–eosin staining

After the administration periods in different groups, rats were deeply anesthetized by the injection of 1% sodium pentobarbital solution, followed by intracardiac injection of 0.9% normal saline and 4% PFA (paraformaldehyde) to flush the blood and fix the tissue. The organs of the rats were fixed, dehydrated, immersed in wax, embedded and sectioned. Paraffin sections of organs were obtained and stained with H&E. The changes in the organ sections were observed to evaluate the safety of the nanopreparations.

2.8. Statistical analysis

All values of statistical analysis are expressed as the mean ± standard deviation. The *t*-test was used to assess significant differences between groups, and SPSS statistical software (SPSS 22.0, SPSS Inc., Chicago, IL, USA) was used for statistical analysis, while $P < 0.05$ and $P < 0.01$ were considered as difference levels of statistical significance.

3. Results and discussion

3.1. Preparation and characterization of HSn and CS-HSn

A diagram of the preparation scheme of CS-HSn and its mechanism of action to promote gastrointestinal absorption is shown in Scheme 1. HSn was prepared by a hydrothermal method and considered a good drug delivery vehicle due to its high drug loading capacity. Subsequently, HSn was encapsulated using CS to increase the internalized absorption of the drug in the intestinal tissues. The uptake pathways of CS-HSn by the intestine were mainly the transmembrane pathway and the cellular bypass pathway. Small intestinal cell uptake pathways for CS-HSn with Clathrin and Caveolin-mediated endocytosis and large pinocytosis pathways, where Clathrin-mediated and large pinocytosis pathways that serve as receptor-mediated endocytosis pathways (des Rieux et al., 2006), Caveolin located on the basal surface of intestinal epithelial cells

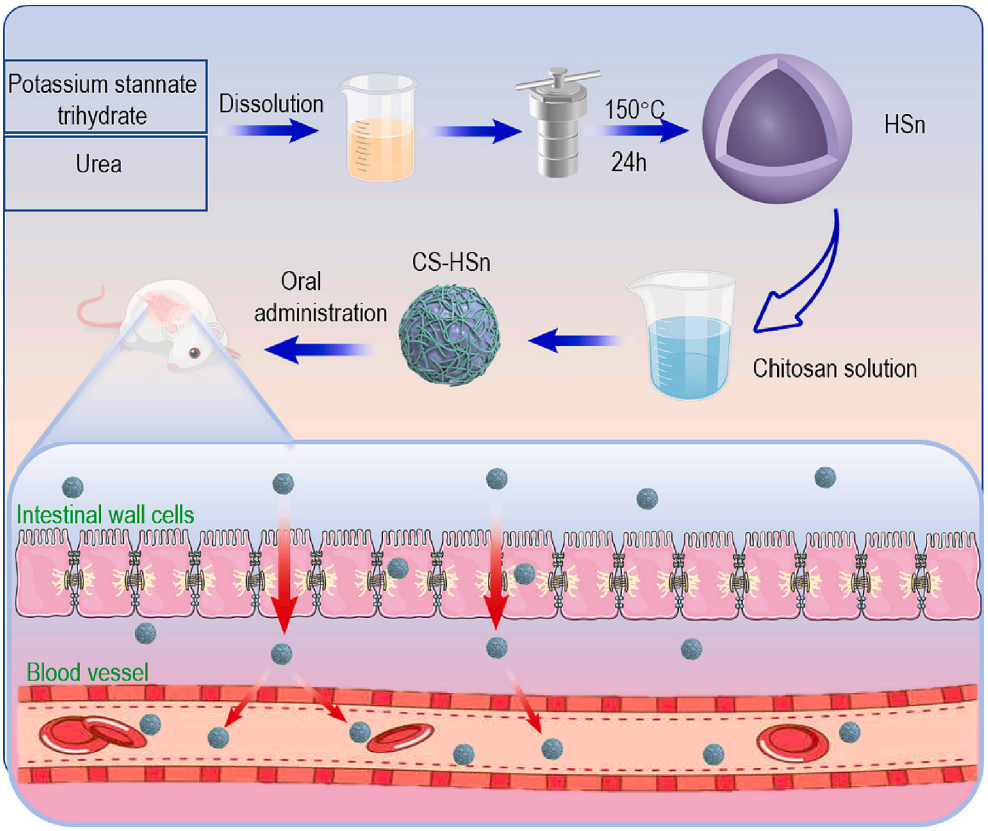

Scheme 1. Scheme diagram of CS-HSn and its mechanism of action to promote gastrointestinal absorption.

and therefore related to drug transport less relevant (Burgos et al., 2004). The absorption of nanoparticles in the intestine results from the combination of multiple pathways. Cell bypass pathway transport closely correlates with the expression of intercellular tight junction proteins, and CS in CS-HSn that can open intercellular tight junctions can facilitate the overall entry of CS-HSn into the body circulation or release drugs into the body circulation. Intercellular tight junctions account for a relatively small proportion of the small intestinal surface, so most drugs or nanoparticles enter the cells via the transmembrane pathway. CS-HSn successfully loaded FEB by physical adsorption and improved the solubility and oral bioavailability of FEB, exerting better uric acid-lowering effects. As shown in Fig. 1A, the prepared HSn was basically spherical and uniformly dispersed, with particle sizes mainly distributed around 140 nm, and a relatively obvious hollow structure could be seen. The hollow structure of HSn gives it properties such as high loading capacity and multifunctional modification. Based on the remarkable properties of HSn, it can be used to deliver both small-molecule drugs (antibiotics, chemotherapeutic drugs and imaging agents) and macromolecular drugs (proteins/peptides and nucleic acids). HSn was coated with CS modified into CS-HSn, and the structure is shown in Fig. 1B. CS-HSn remained relatively regular and spherical with a thin layer of CS on the surface and good dispersion, with a particle size distribution mainly approximately 145 nm. The results of particle size analysis were consistent with the above TEM results, with the main particle size distribution of 135 ± 3.47 nm for HSn and 140 ± 5.27 nm for CS-HSn (Fig. 1C, D). When CS was coated on the outer layer of HSn, the outer charges of both were neutralized. The zeta potentials of HSn and CS-HSn were − 40.53 ± 0.21 mV and 18.88 ± 0.71 mV, respectively (Fig. 1E). The change in the potential of CS-HSn was attributed to the large amounts of amino groups of CS, which also indicated that CS was successfully encapsulated on the HSn surface. The electrostatic interaction between positively charged CS-HSn and negatively charged small epithelial tissue could increase the retention of CS-HSn on the mucosal surface of the gastrointestinal tract (Davoudi et al., 2021). The nanoscale hollow structure inside CS-HSn resulted in a drug loading of 34.27 ± 2.57% of FEB in CS-HSn. The composition of CS-HSn was detected using energy dispersive X-ray spectroscopy (EDS). The results indicated the presence of C, O and Sn in CS-HSn (Fig. 1F). Among them, C was derived from CS, which also indicated the successful encapsulation of CS. DSC and PXRD analyses were performed to investigate the physical state of FEB in CS-HSn. The DSC curves of FEB, CS-HSn, CS-HSn-FEB and the physical mixture (PM) are shown in Fig. 1G. FEB showed a sharp endothermic peak at 208.81 °C, which is consistent with its intrinsic melting point, indicating that FEB is a crystalline drug. PM also has a clear melting peak at 208.81 °C, which is related to the melting of FEB, indicating no change in the physical form of FEB. In contrast, the thermal spectral curves of CS-HSn and CS-HSn-FEB showed no obvious endothermic peaks. This indicates that FEB exists in the CS-HSn-FEB system in an amorphous state. PXRD analysis was performed to further investigate the physical state of FEB, and the obtained PXRD curves are shown in Fig. 1H. FEB has characteristic diffraction peaks at 6.66°, 7.16°, 12.78°, 15.62°, 25.86°, and 26.68°, indicating that FEB is highly crystalline and that the FEB characteristic diffraction peak is still present in PM. CS-HSn and CS-HSn-FEB have characteristic peaks at 27°, 34°, and 52°, and CS-HSn-FEB does not show the characteristic diffraction peak of FEB, suggesting that FEB exists in the CS-HSn-FEB system in an amorphous state. These results are consistent with the DSC results. FEB in an amorphous state can significantly improve the solubility, dissolution rate and oral bioavailability of drugs, and its use is a common method to improve the physicochemical properties of insoluble drugs. As a water-insoluble drug, FEB exhibited a slow release rate throughout its release process, with a cumulative release rate of 6.62 ± 2.00% for FEB in 1 h (Fig. 1I). The cumulative release was low and could not produce the expected therapeutic effect. HSn-FEB exhibited the fastest release rate and higher release amount, with a cumulative release rate of 65.10 ± 4.93% for HSn-FEB in 1 h, which indicates that it is the

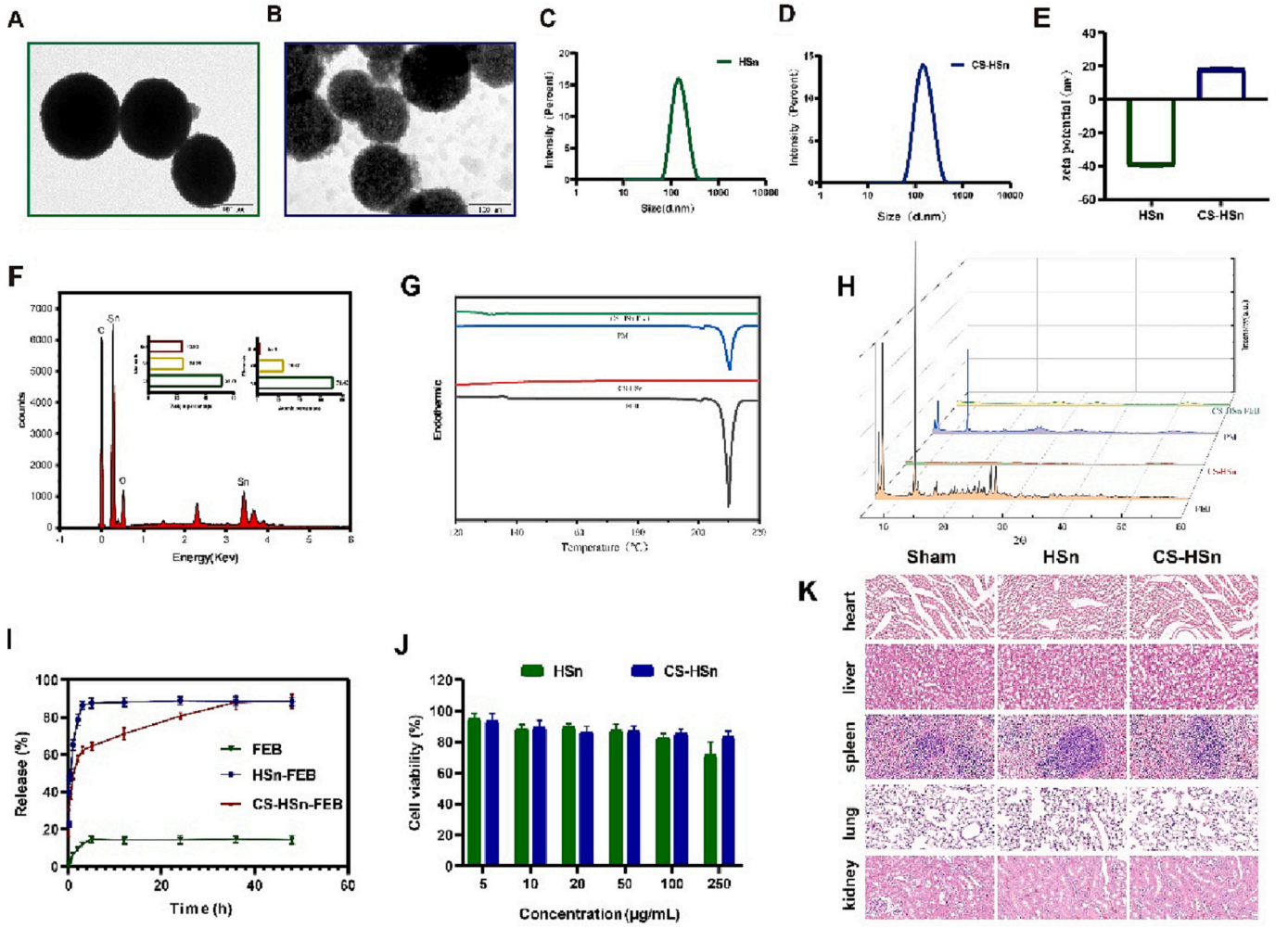

Fig. 1. Preparation and characterization of HSn and CS-HSn. The TEM images of (A) HSn and (B) CS-HSn. The particle size distribution of HSn (C) and CS-HSn (D). (E) The Zeta potential of HSn and CS-HSn. (F) The element spectrum of CS-HSn. (G) The DSC patterns of FEB, CS-HSn, CS-HSn-FEB and PM. (H) The PXRD patterns of FEB, CS-HSn, CS-HSn-FEB and PM. (I) Drug release curves of CS-HSn-FEB, HSn-FEB and FEB. (J) The cytotoxicity of HSn and CS-HSn on Caco-2 cells. (K) H&E staining of heart, liver, spleen, lung and kidney tissue sections of each group for safety evaluation. All data represented the mean ± standard deviation ($n = 3$). $^{*}P < 0.5$, $^{**}P < 0.01$, $^{***}P < 0.001$.

effect of the HSn carrier that greatly increases the solubility and dissolution rate of FEB, mainly due to the change in the presence state of FEB loaded with HSn from the crystalline to the amorphous state, which promoted the dissolution of FEB. After CS modification, the release behavior of FEB from nanoparticles exhibited a relatively slow and sustained release, with a cumulative release rate of 48.50 ± 3.17% in the first 1 h. The reason is that the large amount of release medium first dissolves the FEB adsorbed on the nanoparticle surface, leading to the rapid release of FEB within 1 h. Then, the internal FEB release from the nanoparticles needs to overcome the blockage of the CS encapsulated on the nanoparticle surface and exhibits a slow release. Eventually, with time, the CS will all dissolve, and the loaded FEB will all be released. The slow release of FEB can improve drug bioavailability and enhance therapeutic effects. The safety of the preparation was considered first, and the effect of HSn and CS-HSn on the proliferation of Caco-2 cells cultured in vitro was observed by CCK-8 assay. As shown in Fig. 1J, the cytotoxicity of both HSn and CS-HSn showed concentration-dependent behavior. However, cell viability was still higher than 80% after 24 h of incubation with 100 mg/mL HSn and CS-HSn nanoparticles. The results clearly showed that HSn and CS-HSn had no significant cytotoxicity. In addition, H&E staining results of rat heart, liver, spleen, lung and kidney were collected in Fig. 1K. There was no significant difference in the staining results of orally administered CS-HSn compared with the control group, indicating that CS-HSn has excellent biological safety.

3.2. *In vivo biodistribution and in vitro cell internalization profiles of CS-HSn*

The Caco-2 cell uptake capacity of CS-HSn and its intestinal distribution in vivo were assessed by in vitro cell uptake and in vivo distribution imaging assays (Peng et al., 2015). The small intestine is an important site of absorption for oral drug delivery, and its role as an important biological barrier also affects the absorption of orally administered drugs (Dünnhaupt et al., 2015; Zhao et al., 2022a, 2022b). The tight junctions between small intestinal epithelial cells are closely related to the integrity of the small intestinal epithelial tissue, which is composed of a series of adhesion molecules, transmembrane proteins and regulatory proteins (Welling, 1984; Laukoetter et al., 2006). Opening the tight junctions between cells is an important means to promote drug absorption by facilitating the bypass transit of drugs (Anderberg et al., 1993). In addition, the mucus layer on the intestinal surface is a barrier that affects drug absorption (Gustafsson and Johansson, 2022; Johansson et al., 2013). The mucus layer is negatively charged, which leads to electrostatic repulsion of negatively charged nanoparticles and drug molecules from the surface and affects intestinal absorption (George and Abraham, 2006). Therefore, the modification of

nanoparticles with negatively charged surfaces can also increase the intestinal absorption of drugs. Previous studies have shown that CS has a role in bioadhesion and opening tight junctions between cells in the small intestine (Lang et al., 2020; van der Lubben et al., 2001). Compared to HSn, the altered surface charge of CS-HSn also increases its adhesion capacity. The uptake capacity of Caco-2 cells for CS-HSn was examined using confocal microscopy (CLSM). In Fig. 2A, C, the cellular uptake of CS-HSn was significantly higher than that of HSn by a factor of approximately 2.5, indicating that CS encapsulation could improve the cellular internalization of HSn. To further verify the uptake effect of Caco-2, the uptake of CS-HSn was examined at different time periods. The uptake of CS-HSn by Caco-2 cells showed (Fig. 2B, D) a significant time dependence, in which the uptake rate at 2 h was significantly higher than that at 1 h by approximately 2.17-fold. The intestinal uptake of CS-HSn was further verified by in vivo imaging of small animals. The results showed (Fig. 2E) that both HSn and CS-HSn had significant accumulation in the small intestine. Compared with HSn, CS-HSn was detected with stronger fluorescence intensity, which demonstrated the ability of CS to promote the intestinal uptake of HSn. We also observed in Fig. 2E that stronger fluorescence signals were observed in the liver and kidney of the CS-HSn and HSn experimental groups, indicating that the metabolic process was mainly hepatic and renal. In conclusion, CS promotes the cellular uptake and intestinal internalization of HSn, and CS-HSn has great potential to improve the oral bioavailability of insoluble drugs.

3.3. Absorption of FITC-labeled nanoparticles in the rat intestine

Drug absorption in the intestine occurs mainly through the cellular bypass pathway and the transmembrane absorption pathway, while the cellular bypass pathway is mainly associated with tight junctions (George and Abraham, 2006). However, tight junctions account for a smaller proportion in the small intestinal epithelium, so transmembrane absorption is still the main route of drug absorption (Salah et al., 2020). In previous experiments (Fig. 2A), it was demonstrated that CS could increase the uptake and transport of HSn by Caco-2 cells. Next, we observed the intestinal distribution of HSn and CS-HSn in each intestinal segment (ileum, jejunum and duodenum) by fluorescence microscopy at different time points. As shown in Fig. 3, a large number of nanoparticles (green) were detected in the intestine 2 and 4 h after administration, which also indicated that HSn and CS-HSn could be internalized by intestinal cells. Compared to HSn, the uptake of CS-HSn was significantly stronger in the tissues of different intestinal segments (Fig. 3A). The fluorescence results at different times (2 h and 4 h) also indicated that the intestinal uptake of CS-HSn was significantly time dependent. The fluorescence intensity in different intestinal tissues was significantly enhanced at 4 h compared to 2 h (Fig. 3E). Quantification of the above fluorescence images (Fig. 3B-D, 3F-H) further showed that CS modification observably enhanced the distribution of HSn in the intestine. These results demonstrate that CS-HSn can be used as a drug carrier to enhance the oral bioavailability of FEB.

3.4. Rat pharmacokinetic study and effect of CS-HSn-FEB on UA level

The mean plasma concentration-time profiles of FEB, HSn-FEB and CS-HSn-FEB by oral administration are shown in Fig. 4A. Compared with FEB, CS-HSn-FEB showed significantly higher plasma concentration levels after oral administration. Specifically, the $AUC_{(0\text{-}T)}$ values of FEB, HSn-FEB and CS-HSn-FEB were 39.64 ± 8.85 mg/L*h, 60.48 ± 34.78 mg/L*h and 113.07 ± 9.75 mg/L*h, respectively. Compared with the $AUC_{(0\text{-}T)}$ values of FEB, the $AUC_{(0\text{-}T)}$ of CS-HSn-FEB was 2.90 times higher than that of FEB. This suggests that CS-HSn has advantages in improving intestinal absorption and oral bioavailability. FEB is an inhibitor of nonpurine xanthine oxidase and inhibits both oxidative and reductive xanthine oxidase, enhancing the uric acid-lowering effect of FEB with an oral drug delivery system based on CS-HSn-FEB (Hair et al.,

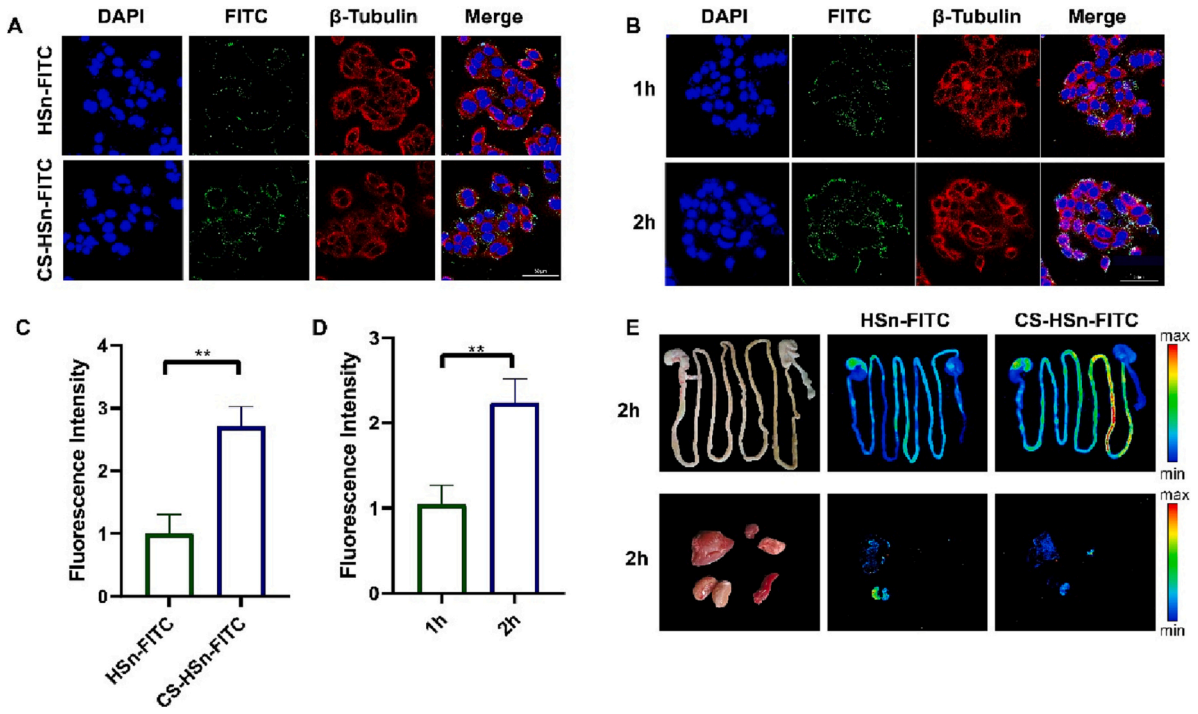

Fig. 2. In vivo bio-distribution and in vitro cell internalization profiles of CS-HSn. (A) CLSM imaging of Caco-2 cells treated with HSn and CS-HSn at 40 min. Nucleus (blue), and cell cytoskeleton (red). All images have a scale of 50 μm. (B) CLSM imaging of Caco-2 cells treated with CS-HSn at 1 h and 2 h. nucleus (blue), and cell cytoskeleton (red). All images have a scale of 50 μm. (C) Fluorescence quantitative analysis of HSn and CS-HSn (green) in Caco-2 cells. (D) Fluorescence quantitative analysis of CS-HSn (green) in Caco-2 cells. (E) Fluorescence imaging of intestinal tissues and vital organs (heart, liver, spleen, lung and kidney) in rats 2 h after oral administration of HSn and CS-HSn. All data represented the mean ± standard deviation ($n = 3$). $^{*}P < 0.5$, $^{**}P < 0.01$, $^{***}P < 0.001$. (For interpretation of the references to colour in this figure legend, the reader is referred to the web version of this article.)

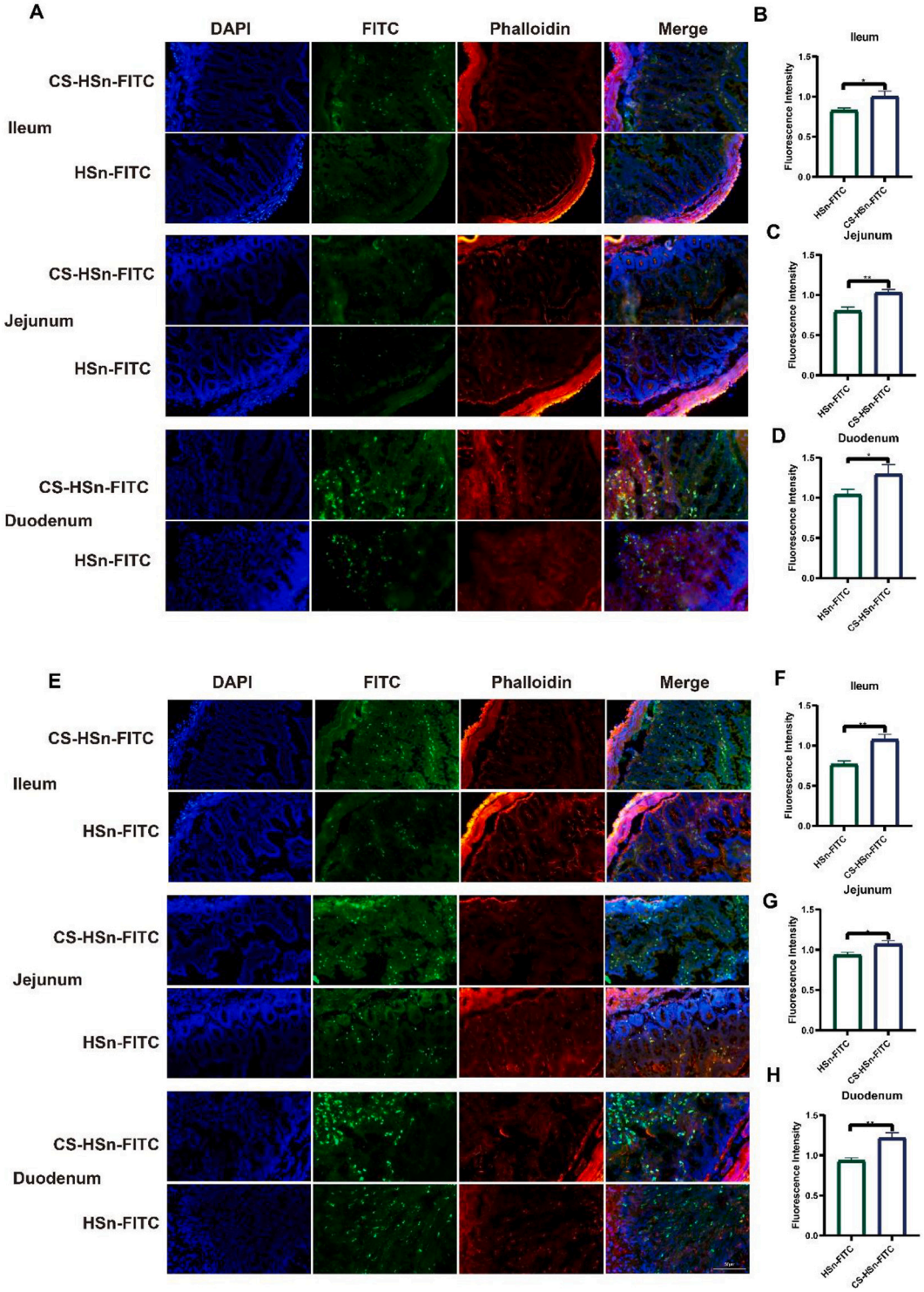

Fig. 3. Absorption of FITC labeled nanoparticles in rat intestine. Fluorescence images of rat intestinal fluorescent labels HSn-FITC and CSn-FITC (green). (A) Fluorescence images of jejunum, ileum and duodenum 2 h after oral administration. (B-D) Quantitative fluorescence statistics after 2 h. (E) Fluorescence images of jejunum, ileum and duodenum 4 h after oral administration. (F-H) Quantitative fluorescence statistics after 4 h. Sections were stained with Rhodamin-phalloidin (red) and DAPI (blue). All data represented the mean ± standard deviation (n = 3). *P < 0.5, **P < 0.01, ***P < 0.001.

2008; Frampton, 2015). In hyperuricemic rats (Wei et al., 2022; Li et al., 2018), compared with the normal group, uric acid levels were significantly higher in the control (hyperuricemic group), FEB-treated and CS-HSn-FEB-treated groups at 1 h (Fig. 4B). Compared with the control group, FEB and CS-HSn-FEB treatment significantly reduced serum uric acid levels after administration, but CS-HSn-FEB was more effective in lowering uric acid levels. The application of CS-HSn-FEB to lower uric acid has great potential.

4. Conclusion

FEB is not well absorbed in the body due to its low solubility. Accordingly, CS-HSn-FEB complexes were prepared for the first time to improve the oral bioavailability of FEB and were characterized by

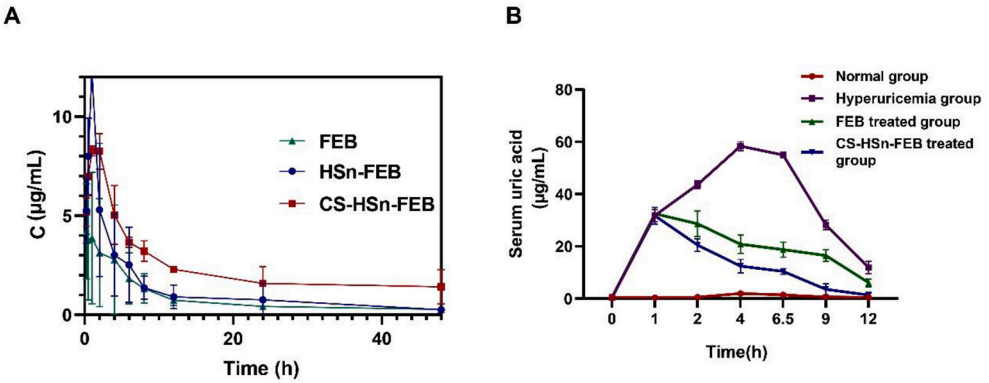

Fig. 4.. Rat pharmacokinetic study and effect of CS-HSn-FEB on UA level. (A)The plasma concentration-time curves of CS-HSn-FEB, HSn-FEB and FEB. (B) Serum uric acid level-time curves of rats under different Treatment. All data represented the mean ± standard deviation (n = 3). *P < 0.5, **P < 0.01, ***P < 0.001.

transmission electron microscopy, particle size and potential. In vitro release and in vivo pharmacokinetic results showed that CS-HSn-FEB significantly increased the dissolution rate of FEB and improved oral bioavailability. CS modification also greatly improved the internalization of nanoparticles in intestinal tissues and enhanced the anti-uric acid therapeutic effect of FEB. In this study, CS-HSn was successfully proven to have excellent physical and chemical properties and broad application prospects in oral absorption therapy.

CRediT authorship contribution statement

Junpeng Sun: Conceptualization, Data curation, Formal analysis, Investigation, Methodology, Resources, Supervision, Validation, Visualization, Writing – original draft. **Jiaqun Du:** Data curation, Conceptualization, Methodology. **Xiaobang Liu:** Methodology, Writing – original draft. **Jinyu An:** Methodology. **Yingqiao Li:** Methodology. **Yanan Yu:** Data curation. **Minghui Li:** Software, Methodology. **Li Zheng:** Methodology. **Chao Wu:** Funding acquisition. **Lili Hu:** Funding acquisition, Writing – review & editing.

Declaration of Competing Interest

The authors declare no competing financial interest. The manuscript was written through contributions of all authors. All authors have given approval to the final version of the manuscript.

Data availability

The raw/processed data required to reproduce these findings cannot be shared at this time as the data also forms part of an ongoing study.

Acknowledgments

The authors acknowledge the financial support received from the Natural Science Foundation of Liaoning Province (Nos.20180550155, 2021-MS-332), Scientific Research Project of the Educational Department of Liaoning Province (Nos.JYTQN201917, JYTQN201919, JYTJCZR2020070, LJKMZ20222081), Liaoning Provincial Key Laboratory of Marine Bioactive Substances and Technological Innovation Center of Liaoning Pharmaceutical Action and Quality Evaluation (Nos. 2022-8, 2022-12, 2022-13), Application Research Project of Jinzhou Medical University (Nos.H2021024), Scientific and technological projects of jinzhou city (Nos. JZ2022B042).

References

Anderberg, E.K., Lindmark, T., Artursson, P., 1993. Sodium caprate elicits dilatations in human intestinal tight junctions and enhances drug absorption by the paracellular route. Pharm. Res. 10 (6), 857–864. https://doi.org/10.1023/a:1018909210879.

Bai, A., Wu, C., Liu, X., Lv, H., Xu, X., Cao, Y., Shang, W., Hu, L., Liu, Y., 2018. Development of a tin oxide carrier with mesoporous structure for improving the dissolution rate and oral relative bioavailability of fenofibrate. Drug Design, Develop. Therapy 12, 2129–2138. https://doi.org/10.2147/DDDT.S166989.

Becker, M.A., Schumacher Jr., H.R., Wortmann, R.L., MacDonald, P.A., Eustace, D., Palo, W.A., Streit, J., Joseph-Ridge, N., 2005. Febuxostat compared with allopurinol in patients with hyperuricemia and gout. N. Engl. J. Med. 353 (23), 2450–2461. https://doi.org/10.1056/NEJMoa050373.

Bernkop-Schnürch, A., Dünnhaupt, S., 2012. Chitosan-based drug delivery systems. Eur. J. Pharm. Biopharm. 81 (3), 463–469. https://doi.org/10.1016/j.ejpb.2012.04.007.

Bonferoni, M.C., Sandri, G., Rossi, S., Ferrari, F., Caramella, C., 2009. Chitosan and its salts for mucosal and transmucosal delivery. Exp. Opin. Drug Deliv. 6 (9), 923–939. https://doi.org/10.1517/17425240903114142.

Burgos, P.V., Klattenhoff, C., de la Fuente, E., Rigotti, A., González, A., 2004. Cholesterol depletion induces PKA-mediated basolateral-to-apical transcytosis of the scavenger receptor class B type I in MDCK cells. Proc. Natl. Acad. Sci. U. S. A. 101 (11), 3845–3850. https://doi.org/10.1073/pnas.0400295101.

Davoudi, Z., Peroutka-Bigus, N., Bellaire, B., Jergens, A., Wannemuehler, M., Wang, Q., 2021. Gut organoid as a new platform to study alginate and chitosan mediated PLGA nanoparticles for drug delivery. Marine Drugs 19 (5), 282. https://doi.org/10.3390/md19050282.

Dehlin, M., Jacobsson, L., Roddy, E., 2020. Global epidemiology of gout: prevalence, incidence, treatment patterns and risk factors. Nat. Rev. Rheumatol. 16 (7), 380–390. https://doi.org/10.1038/s41584-020-0441-1.

des Rieux, A., Fievez, V., Garinot, M., Schneider, Y.J., Préat, V., 2006. Nanoparticles as potential oral delivery systems of proteins and vaccines: a mechanistic approach. J. Control. Release. 116 (1), 1–27. https://doi.org/10.1016/j.jconrel.2006.08.013.

Dou, T., Wang, J., Han, C., Shao, X., Zhang, J., Lu, W., 2019. Cellular uptake and transport characteristics of chitosan modified nanoparticles in Caco-2 cell monolayers. Int. J. Biol. Macromol. 138, 791–799. https://doi.org/10.1016/j.ijbiomac.2019.07.168.

Dünnhaupt, S., Kammona, O., Waldner, C., Kiparissides, C., Bernkop-Schnürch, A., 2015. Nano-carrier systems: strategies to overcome the mucus gel barrier. Eur. J. Pharm. Biopharm. 96, 447–453. https://doi.org/10.1016/j.ejpb.2015.01.022.

Ejsmont, A., Stasiłowicz-Krzemień, A., Ludowicz, D., Cielecka-Piontek, J., Goscianska, J., 2021. Synthesis and characterization of nanoporous carbon carriers for losartan potassium delivery. Materials (Basel, Switzerland) 14 (23), 7345. https://doi.org/10.3390/ma14237345.

Foote, M., 2007. Using nanotechnology to improve the characteristics of antineoplastic drugs: improved characteristics of nab-paclitaxel compared with solvent-based paclitaxel. Biotechnol. Annu. Rev. 13, 345–357. https://doi.org/10.1016/S1387-2656(07)13012-X.

Frampton, J.E., 2015. Febuxostat: a review of its use in the treatment of hyperuricaemia in patients with gout. Drugs 75 (4), 427–438. https://doi.org/10.1007/s40265-015-0360-7.

George, M., Abraham, T.E., 2006. Polyionic hydrocolloids for the intestinal delivery of protein drugs: alginate and chitosan–a review. J. Control. Release. 114 (1), 1–14. https://doi.org/10.1016/j.jconrel.2006.04.017.

Ghahfarokhi, M.R., Dini, G., Movahedi, B., 2022. Fabrication of chitosan-coated mesoporous silica nanoparticles bearing rosuvastatin as a drug delivery system. Curr. Drug Deliv. 19 (1), 64–73. https://doi.org/10.2174/1567201818666210609165630.

Gupta, S.S., Sabharwal, N., Patti, R., Kupfer, Y., 2019. Allopurinol-induced stevens-johnson syndrome. Am J Med Sci 357 (4), 348–351. https://doi.org/10.1016/j.amjms.2018.11.018.

Gustafsson, J.K., Johansson, M.E.V., 2022. The role of goblet cells and mucus in intestinal homeostasis. Nat. Rev. Gastroenterol. Hepatol. 19 (12), 785–803. https://doi.org/10.1038/s41575-022-00675-x.

Habib, B.A., Abd El-Samiae, A.S., El-Houssieny, B.M., Tag, R., 2021. Formulation, characterization, optimization, and in-vivo performance of febuxostat self-nano-emulsifying system loaded sublingual films. Drug Deliv. 28 (1), 1321–1333. https://doi.org/10.1080/10717544.2021.1927247.

Hair, P.I., McCormack, P.L., Keating, G.M., 2008. Febuxostat. Drugs 68 (13), 1865–1874. https://doi.org/10.2165/00003495-200868130-00006.
Hu, M., Li, Y., Decker, E.A., Xiao, H., McClements, D.J., 2010. Influence of tripolyphosphate cross-linking on the physical stability and lipase digestibility of chitosan-coated lipid droplets. J. Agric. Food Chem. 58 (2), 1283–1289. https://doi.org/10.1021/jf903270y.
Hu, C.S., Chiang, C.H., Hong, P.D., Yeh, M.K., 2012. Influence of charge on FITC-BSA-loaded chondroitin sulfate-chitosan nanoparticles upon cell uptake in human Caco-2 cell monolayers. Int. J. Nanomedicine 7, 4861–4872. https://doi.org/10.2147/IJN.S34770.
Huong, P.T., Ha, T.N., Nhu, T.T.Q., Nga, N.T.H., Anh Jr., N.H., Hoa, V.D., Binh, N.Q., Anh, N.H., 2022. Allopurinol-induced Stevens-Johnson syndrome and toxic epidermal necrolysis: Signal detection and preventability from Vietnam National pharmacovigilance database. J. Clin. Pharm. Ther. 47 (12), 2014–2019. https://doi.org/10.1111/jcpt.13740.
Ibrahim, A.H., Smått, J.H., Govardhanam, N.P., Ibrahim, H.M., Ismael, H.R., Afouna, M. I., Samy, A.M., Rosenholm, J.M., 2020. Formulation and optimization of drug-loaded mesoporous silica nanoparticle-based tablets to improve the dissolution rate of the poorly water-soluble drug silymarin. Eur. J. Pharma. Sci. 142, 105103 https://doi.org/10.1016/j.ejps.2019.105103.
Johansson, M.E., Sjövall, H., Hansson, G.C., 2013. The gastrointestinal mucus system in health and disease. Nat. Rev. Gastroenterol. Hepatol. 10 (6), 352–361. https://doi.org/10.1038/nrgastro.2013.35.
Kimura, Y., Sawai, N., Okuda, H., 2001. Antitumour activity and adverse reactions of combined treatment with chitosan and doxorubicin in tumour-bearing mice. J. Pharm. Pharmacol. 53 (10), 1373–1378. https://doi.org/10.1211/0022357011777873.
Lang, X., Wang, T., Sun, M., Chen, X., Liu, Y., 2020. Advances and applications of chitosan-based nanomaterials as oral delivery carriers: A review. Int. J. Biol. Macromol. 154, 433–445. https://doi.org/10.1016/j.ijbiomac.2020.03.148.
Laukoetter, M.G., Bruewer, M., Nusrat, A., 2006. Regulation of the intestinal epithelial barrier by the apical junctional complex. Curr. Opin. Gastroenterol. 22 (2), 85–89. https://doi.org/10.1097/01.mog.0000203864.48255.4f.
Li, J., Yang, Y., Lu, L., Ma, Q., Zhang, J., 2018. Preparation, characterization and systemic application of self-assembled hydroxyethyl starch nanoparticles-loaded flavonoid Morin for hyperuricemia therapy. Int. J. Nanomedicine 13, 2129–2141. https://doi.org/10.2147/IJN.S158585.
Li, Q., Li, X., Wang, J., Liu, H., Kwong, J.S., Chen, H., Li, L., Chung, S.C., Shah, A., Chen, Y., An, Z., Sun, X., Hemingway, H., Tian, H., Li, S., 2019. Diagnosis and treatment for hyperuricemia and gout: a systematic review of clinical practice guidelines and consensus statements. BMJ Open 9 (8), e026677. https://doi.org/10.1136/bmjopen-2018-026677.
Li, Z., He, Y., Klausen, L.H., Yan, N., Liu, J., Chen, F., Song, W., Dong, M., Zhang, Y., 2020. Growing vertical aligned mesoporous silica thin film on nanoporous substrate for enhanced degradation, drug delivery and bioactivity. Bioactive Mater. 6 (5), 1452–1463. https://doi.org/10.1016/j.bioactmat.2020.10.026.
Liao, J., Peng, H., Liu, C., Li, D., Yin, Y., Lu, B., Zheng, H., Wang, Q., 2021. Dual pH-responsive-charge-reversal micelle platform for enhanced anticancer therapy. Mater. Sci. Eng. C Mater. Biol. Appl. 118, 111527 https://doi.org/10.1016/j.msec.2020.111527.
Londhe, V., Bakshi, P., 2023. Improved oral bioavailability of febuxostat by liquid self-micro emulsifying drug delivery system in capsule shells. Ann. Pharm. Fr. S0003-4509 (23) https://doi.org/10.1016/j.pharma.2023.05.003, 00049–4. Advance online publication.
Lou, L., Subbiah, S., Smith, E., Kendall, R.J., Ramkumar, S.S., 2019. Functional PVA/VB2/TiO2 Nanofiber Webs for Controlled Drug delivery. ACS Appl. Bio. Mater. 2 (12), 5916–5929. https://doi.org/10.1021/acsabm.9b00726.
Major, T.J., Dalbeth, N., Stahl, E.A., Merriman, T.R., 2018. An update on the genetics of hyperuricaemia and gout. Nat. Rev. Rheumatol. 14 (6), 341–353. https://doi.org/10.1038/s41584-018-0004-x.
Nuki, G., Simkin, P.A., 2006. A concise history of gout and hyperuricemia and their treatment. Arthritis Res. Therapy 8 Suppl 1 (Suppl. 1), S1. https://doi.org/10.1186/ar1906.
Peng, H., Wang, C., Xu, X., Yu, C., Wang, Q., 2015. An intestinal Trojan horse for gene delivery. Nanoscale 7 (10), 4354–4360. https://doi.org/10.1039/c4nr06377e.
Sahni, J.K., Chopra, S., Ahmad, F.J., Khar, R.K., 2008. Potential prospects of chitosan derivative trimethyl chitosan chloride (TMC) as a polymeric absorption enhancer: synthesis, characterization and applications. J. Pharm. Pharmacol. 60 (9), 1111–1119. https://doi.org/10.1211/jpp.60.9.0001.
Salah, E., Abouelfetouh, M.M., Pan, Y., Chen, D., Xie, S., 2020. Solid lipid nanoparticles for enhanced oral absorption: A review. Colloids Surf. B: Biointerfaces 196, 111305. https://doi.org/10.1016/j.colsurfb.2020.111305.
Sun, J., Yang, Z., Teng, L., 2020. Nanotechnology and Microtechnology in Drug delivery Systems. Dose-response: Pub. Int. Hormesis Soc. 18 (2) https://doi.org/10.1177/1559325820907810, 1559325820907810.
Tang, F., Li, L., Chen, D., 2012. Mesoporous silica nanoparticles: synthesis, biocompatibility and drug delivery. Adv. Mater. (Deerfield Beach, Fla.) 24 (12), 1504–1534. https://doi.org/10.1002/adma.201104763.
Tong, T., Qi, Y., Bussiere, L.D., Wannemuehler, M., Miller, C.L., Wang, Q., Yu, C., 2020. Transport of artificial virus-like nanocarriers through intestinal monolayers via microfold cells. Nanoscale 12 (30), 16339–16347. https://doi.org/10.1039/d0nr03680c.
van der Lubben, I.M., Verhoef, J.C., Borchard, G., Junginger, H.E., 2001. Chitosan and its derivatives in mucosal drug and vaccine delivery. Eur. J. Pharma. Sci. 14 (3), 201–207. https://doi.org/10.1016/s0928-0987(01)00172-5.
Wang, Q., Zhang, N., Hu, X., Yang, J., Du, Y., 2008. Chitosan/polyethylene glycol blend fibers and their properties for drug controlled release. J. Biomed. Mater. Res. A 85 (4), 881–887. https://doi.org/10.1002/jbm.a.31544.
Wei, C., Wang, Q., Weng, W., Adu-Frimpong, M., Toreniyazov, E., Ji, H., Xu, X., Yu, J., 2022. Enhanced oral bioavailability and anti-hyperuricemic activity of liquiritin via a self-nanoemulsifying drug delivery system. J. Sci. Food Agric. 102 (5), 2032–2040. https://doi.org/10.1002/jsfa.11542.
Welling, P.G., 1984. Interactions affecting drug absorption. Clin. Pharmacokinet. 9 (5), 404–434. https://doi.org/10.2165/00003088-198409050-00002.
Yang, L., Shi, R., Zhao, R., Zhu, Y., Liu, B., Gai, S., Feng, L., 2022. Near-infrared upconversion mesoporous tin dioxide theranostic nanocapsules for synergetic cancer chemophototherapy. ACS Appl. Mater. Interfaces 14 (2), 2650–2662. https://doi.org/10.1021/acsami.1c23174.
Zhang, W., Zhao, M., Gao, Y., Cheng, X., Liu, X., Tang, S., Peng, Y., Wang, N., Hu, D., Peng, H., Zhang, J., Wang, Q., 2022. Biomimetic erythrocytes engineered drug delivery for cancer therapy. Chem. Eng. J. 433 (2022), 133498 https://doi.org/10.1016/j.cej.2021.133498.
Zhao, Z., Chen, X., Dowbaj, A.M., Sljukic, A., Bratlie, K., Lin, L., Fong, E.L.S., Balachander, G.M., Chen, Z., Soragni, A., Huch, M., Zeng, Y.A., Wang, Q., Yu, H., 2022a. Organoids. Nat. Rev. Methods Prim. 2, 94. https://doi.org/10.1038/s43586-022-00174-y.
Zhao, D., Yang, N., Xu, L., Du, J., Yang, Y., Wang, D., 2022b. Hollow structures as drug carriers: recognition, response, and release. Nano Res. 15 (2), 739–757. https://doi.org/10.1007/s12274-021-3595-5.
Zhou, Y., Niu, B., Zhao, Y., Fu, J., Wen, T., Liao, K., Quan, G., Pan, X., Wu, C., 2021. Multifunctional nanoreactors-integrated microneedles for cascade reaction-enhanced cancer therapy. J. Control. Release. 339, 335–349. https://doi.org/10.1016/j.jconrel.2021.09.041.